

# A five-site model for liquid water and the reproduction of the density anomaly by rigid, nonpolarizable potential functions

Michael W. Mahoney

*Department of Physics, Yale University, New Haven, Connecticut 06520*

William L. Jorgensen

*Department of Chemistry, Yale University, New Haven, Connecticut 06520*

(Received 27 October 1999; accepted 29 February 2000)

The ability of simple potential functions to reproduce accurately the density of liquid water from  $-37$  to  $100$  °C at 1 to 10 000 atm has been further explored. The result is the five-site TIP5P model, which yields significantly improved results; the average error in the density over the  $100$ ° temperature range from  $-37.5$  to  $62.5$  °C at 1 atm is only  $0.006$  g cm $^{-3}$ . Classical Monte Carlo statistical mechanics calculations have been performed to optimize the parameters, especially the position of the negative charges along the lone-pair directions. Initial calculations with 216 molecules in the *NPT* ensemble at 1 atm focused on finding a model that reproduced the shape of the liquid density curve as a function of temperature. Calculations performed for 512 molecules with the final TIP5P model demonstrate that the density maximum near  $4$  °C at 1 atm is reproduced, while high-quality structural and thermodynamic results are maintained. Attainment of high precision for the low-temperature runs required sampling for more than 1 billion Monte Carlo configurations. In addition, the dielectric constant was computed from the response to an applied electric field; the result is  $81.5 \pm 1.5$  at  $25$  °C and the experimental curve is mirrored from  $0$ – $100$  °C at 1 atm. The TIP5P model is also found to perform well as a function of pressure; the density of liquid water at  $25$  °C is reproduced with an average error of  $\sim 2\%$  over the range from 1 to 10 000 atm, and the shift of the temperature of maximum density to lower temperature with increasing pressure is also obtained. © 2000 American Institute of Physics. [S0021-9606(00)50820-4]

## I. INTRODUCTION

Prior to 1983, Monte Carlo (MC) and molecular dynamics (MD) calculations for liquid water generally used the BNS, MCY, and ST2 potential functions.<sup>1</sup> In 1983 the TIP3P and TIP4P models<sup>2,3</sup> were introduced and, along with the SPC<sup>4</sup> and SPC/E models,<sup>5</sup> are the most commonly used water models today. These models, along with the ST2 model,<sup>6</sup> were developed in conjunction with liquid-state calculations, generally at  $25$  °C. The models have been used successfully to study a wide variety of properties of liquid water, often at conditions far from their original parameterization.<sup>7</sup> Among the most well known of the peculiar properties of liquid water is the behavior of its density as a function of temperature and pressure,  $\rho(T, P)$ . Liquid water at standard pressure exhibits a temperature of maximum density (TMD) at  $4.0$  °C and its density is nearly constant between  $-15$  and  $+25$  °C.<sup>8–10</sup> Notably, none of the commonly used water models is successful at reproducing  $\rho(T)$  well in the temperature region of interest.<sup>11–13</sup> Several models have been reported to yield a density maximum,<sup>6,12–17</sup> although questions about the convergence of some of the earlier calculations have been raised.<sup>13,18</sup> In particular the ST2 model has been reported to have a density maximum near  $27$ <sup>6</sup> or  $40$  °C<sup>12(a)</sup> and SPC/E has a TMD near  $-38$  °C.<sup>14</sup> The polarizable PPC has been reported to have a density maximum near the correct value in moderate length molecular dynamics calculations at zero pressure (*vide infra*).<sup>16</sup> TIP4P water has been found to have a density maximum near  $-13$ <sup>12(b),(c)</sup>

or  $-23$  °C<sup>15</sup> by demonstrating that it possesses a minimum in its pressure as a function of temperature along an isochore. More recently, long MC calculations with the TIP4P model in the isothermal–isobaric (*NPT*) ensemble located the TMD near  $-15$  °C and, in addition, a region of nearly constant density is found between  $-35$  and  $0$  °C.<sup>13</sup> Thus, although the qualitative feature of a density maximum exists for several of the simple water models, quantitative agreement is lacking, and the shape of  $\rho(T)$  has also not been well reproduced.

Numerous attempts have been made to improve potential functions for liquid water. The addition of bond flexibility,<sup>19–24</sup> variable electronic degrees of freedom,<sup>16,17,23,24</sup> and more complex functional forms<sup>17,19,24</sup> are examples. Given that most flexible models do not properly describe the dependence of the change in dipole moment on molecular geometry,<sup>19,20,25–27</sup> and suggestions that geometric flexibility should be included only in polarizable models,<sup>21,23</sup> we have continued to explore rigid models. While much work is currently being done to include electronic polarization, the computational expense of adding many-body terms, in particular given the long calculations required to obtain convergence of computed properties at low temperatures, coupled with unresolved questions about the optimal method of including polarization and the effects of incomplete iteration,<sup>16,28–32</sup> led us to focus efforts on further optimization of fixed-charge models. Additional refinement of three- and four-site models was not fruitful, so five-site models were pursued, while still retaining the computationally efficient Coulomb plus 12-6

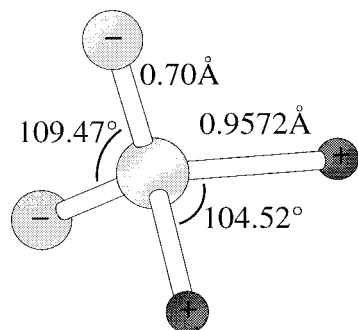


FIG. 1. TIP5P monomer geometry.

Lennard-Jones form. Departure from the latter would be problematic for use in conjunction with standard force fields for organic and biomolecular systems. The ST2 model is the most successful prior five-site model<sup>6</sup>; however, it uses a cubic scaling function to dampen the short-range electrostatic interactions and yields an overly structured liquid with a density error of 8% at 25 °C and 1 atm and an overly high TMD, as noted above. Nevertheless, before resorting to more complex charge distributions, we decided to attempt the optimization of a five-site model that would simultaneously eliminate the scaling function, yield improved density results including a correct TMD, and not sacrifice performance for other structural or thermodynamic properties in comparison to the TIP4P model. In the process, factors that control the position of the TMD would emerge, though at considerable computational expense owing to the need to obtain the density profile with alternative parameter sets.

The next section presents the potential function, followed in Sec. III by computational details. In Secs. IV and V the temperature dependence of several thermodynamic and dielectric properties, the liquid's structure, and energy distributions are presented for the TIP5P model. Section VI covers the results of the MC simulations at elevated pressures, properties of the water dimer are noted in Sec. VII, and Sec. VIII describes observations and decisions that were made in the course of optimizing the model and the behavior of related models as a function of temperature. Sections IX and X contain further discussion and the conclusion.

## II. FORM OF THE TIP5P POTENTIAL FUNCTION

Details on the optimization procedure and analysis of some aspects of intermediate models may be found in Sec. VIII. The geometry of the TIP5P model is depicted in Fig. 1, and its parameters are presented in Table I, along with those for the TIP3P and TIP4P models. For all TIP $n$ P models, the OH bond length,  $r_{\text{OH}}$ , and HOH bond angle,  $\theta_{\text{HOH}}$ , have been set to the experimental gas-phase values, i.e., 0.9572 Å and 104.52°. For TIP5P, the negatively charged interaction sites are located symmetrically along the lone-pair directions with an intervening angle,  $\theta_{\text{LOL}}$ , of 109.47°. A charge of +0.241  $e$  is placed on each hydrogen site, and charges of equal magnitude and opposite sign are placed on the lone-pair interaction sites. The dipole moments are 2.35, 2.18, and 2.29 D for TIP3P, TIP4P, and TIP5P, respectively. There is no charge on oxygen for TIP5P; however, the only Lennard-

TABLE I. Monomer geometry and parameters for the TIP $n$ P potential functions.

	TIP3P	TIP4P	TIP5P
$q_H$ ( $e$ )	0.417	0.520	0.241
$\sigma_0$ (Å)	3.150 61	3.153 65	3.12
$\epsilon_0$ (kcal/mol)	0.1521	0.1550	0.16
$r_{\text{OH}}$ (Å)	0.9572	0.9572	0.9572
$\theta_{\text{HOH}}$ (deg)	104.52	104.52	104.52
$r_{\text{OL}}$ (Å)		0.15	0.70
$\theta_{\text{LOL}}$ (deg)			109.47

Jones potential operates between oxygens with a  $\sigma_0$  of 3.12 Å and an  $\epsilon_0$  of 0.16 kcal/mol. The potential energy between two water molecules,  $a$  and  $b$ , is then given by Eq. (1), where  $i$  and  $j$  are the charged sites on  $a$  and  $b$ , respectively, and  $r_{\text{OO}}$  is the oxygen—oxygen distance,

$$E_{ab} = \sum_{ij} \frac{q_i q_j e^2}{r_{ij}} + 4\epsilon_0 \left[ \left( \frac{\sigma_0}{r_{\text{OO}}} \right)^{12} - \left( \frac{\sigma_0}{r_{\text{OO}}} \right)^6 \right]. \quad (1)$$

## III. COMPUTATIONAL DETAILS

Monte Carlo statistical mechanical calculations were performed on the TIP5P model in the isothermal-isobaric ensemble at a pressure of 1 atm at temperatures every 12.5 °C between −37.5 and 75.0 °C. In addition, calculations at a range of elevated pressures up to 10 000 atm were performed. As pointed out previously,<sup>13</sup>  $NPT$  MC calculations are a good choice for computing liquid densities because there is no uncertainty in the implementation of the ensemble, and because the temperature and pressure controls are exact. Periodic boundary conditions were used with a cubic sample of 512 water molecules with 9 Å spherical cutoffs based on the OO separation,  $r_{\text{OO}}$ . The starting coordinates for each calculation came from a box equilibrated at either 25 °C and 1 atm or at closer conditions. Volume changes were attempted approximately every 2000 configurations, and their magnitude as well as the ranges for molecular translations and rotations were adjusted to yield acceptance rates of approximately 40% for new configurations.

Table II(a) lists the lengths of the equilibration and averaging periods for the MC simulations at standard pressure, and Table II(b) does the same for the calculations at elevated pressures. The radial distribution functions, potential energy, and volume are converged to within ~1% in runs of a few million MC configurations at 25 °C and 1 atm.<sup>13,33,34</sup> The present calculations were far longer owing to much slower convergence at low temperatures and the need for particularly precise results to locate the temperature of maximum density in the relatively flat region near where  $d\rho/dT=0$ .

The density is calculated from the average volume with Eq. (2), where  $\rho$  is the

$$\rho = M / (0.6022 * V / N) \quad (2)$$

density in  $\text{g cm}^{-3}$ ,  $M$  is the molecular weight,  $N$  is the number of molecules in the periodic box,  $V$  is the calculated volume in Å<sup>3</sup>, and 0.6022 is the unit conversion factor. The heat of vaporization is well approximated from the calculated energy via Eq. (3),<sup>3</sup> where  $R$

TABLE II. (a) Lengths of Monte Carlo simulations with 512 molecules for TIP5P water at (a) 1 atm., (b) elevated pressures. (c) Lengths of Monte Carlo simulations with 216 molecules for TIP5P water at 1 atm, which were used to compute the dielectric constants.

(a)			
$T$ (°C)		Equil. <sup>a</sup>	Average <sup>a</sup>
-37.5		400	1000
-25.0		300	1000
-12.5		300	1000
0.0		100	500
12.5		100	400
25.0		50	250
37.5		50	200
50.0		50	150
62.5		50	150
75.0		50	150
(b)			
$T$ (°C)	$P$ (atm)	Equil. <sup>a</sup>	Average <sup>a</sup>
-25.0	1000	200	600
-12.5	1000	200	600
0.0	1000	100	500
12.5	1000	50	300
25.0	1000	50	150
-37.5	2000	400	600
-25.0	2000	400	600
-12.5	2000	300	500
0.0	2000	100	300
12.5	2000	50	250
25.0	2000	50	150
25.0	3000	10	40
25.0	4000	10	40
25.0	5000	10	40
25.0	6000	10	40
25.0	8000	10	40
25.0	10 000	10	40
(c)			
$T$ (°C)		Equil. <sup>a</sup>	Average <sup>a</sup>
0.0		200	500
25.0		50	400
50.0		50	250
75.0		50	250
100.0		50	250

<sup>a</sup>Millions of MC steps.

$$\Delta H_{\text{vap}} \approx -E_{\text{liq}}/N + RT \quad (3)$$

is the gas constant and  $T$  is the absolute temperature. The heat capacity, isothermal compressibility, and coefficient of thermal expansion were calculated from standard fluctuation formulas, and also by numerical differentiation.<sup>34</sup>

Calculations were also performed for the dielectric constant at 1 atm every 25.0 °C between 0.0 and 100.0 °C. The calculations involved applying a nonsaturating electric field across the simulation box and measuring the average system dipole moment along the direction of the applied field. Details are similar to calculations performed previously,<sup>35</sup> and involved 216 molecules subjected to NVT MC calculations with the density set to the experimental value at that temperature, truncation of intermolecular interactions at  $r_{\text{OO}}=8 \text{ \AA}$ , and the use of a reaction field to treat the long-range interactions. The dielectric constant  $\epsilon$  is calculated from Eq. (4), where  $E_0$  is the applied

$$\left(\frac{4\pi}{3}\right) \frac{\langle P \rangle}{E_0} = \left(\frac{\epsilon-1}{3}\right) \frac{2\epsilon_{\text{RF}}+1}{2\epsilon_{\text{RF}}+\epsilon} \quad (4)$$

field strength of  $1.5 \times 10^8 \text{ V m}^{-1}$ , the dielectric constant of the reaction field  $\epsilon_{\text{RF}}=\infty$ , and  $\langle P \rangle$  is the calculated system dipole moment per unit volume along the direction of  $E_0$ . Table II(c) lists the lengths of the equilibration and averaging periods for each of the dielectric constant calculations.

All Monte Carlo calculations were performed with the BOSS program, version 3.8;<sup>36</sup> the dielectric constant calculations required modifications, which were tested by successfully reproducing dielectric constants of TIP4P and SPC water.<sup>35</sup> In our current implementation, which is not fully optimized for TIP5P, the MC simulations with an 8.5 Å spherical cutoff require ~55% more computer time with the TIP5P model than with the TIP3P or TIP4P models. Error estimates in the calculated quantities were obtained by the batch-means procedure.<sup>37,38</sup> The batch size was 10 million configurations in all cases; tests with larger batch sizes confirmed the convergence of the error estimates.

#### IV. TEMPERATURE DEPENDENCE OF THERMODYNAMIC AND DIELECTRIC PROPERTIES

The results for thermodynamic properties of the TIP5P model at 25 °C and 1 atm are presented in Table III along with the experimental data<sup>8-10</sup> and the results for the TIP3P and TIP4P models, as previously reported.<sup>13</sup> The density and heat of vaporization for TIP5P water are within a fraction of a percent of the experimental values. The runs are sufficiently long that some fluctuation properties are moderately well converged. Nevertheless, it is still found that better estimates are obtained by numerical differentiation, which was performed here for the isobaric heat capacity,  $C_p$ , and the coefficient of thermal expansion,  $\alpha$ .<sup>13</sup> The  $C_p$  for TIP5P water is somewhat larger than both the experimental value and

TABLE III. Calculated and experimental properties for liquid water at 25 °C and 1 atm.

	TIP3P	TIP4P	TIP5P	Expt. <sup>a</sup>
$\rho$ (g/cm <sup>3</sup> )	1.002±0.001	1.001±0.001	0.999±0.001	0.997
$-E$ (kcal/mol)	9.82±0.01	10.06±0.01	9.87±0.01	9.92
$\Delta H_{\text{vap}}$ (kcal/mol)	10.41±0.01	10.65±0.01	10.46±0.01	10.51
$C_p$ (cal/mol deg)	20.0±0.6	20.4±0.7	29.1±0.8	18.0
$10^6 \kappa$ (atm <sup>-1</sup> )	64±5	60±5	41±2	45.8
$10^5 \alpha$ (deg <sup>-1</sup> )	92±8	44±8	63±6	25.7

<sup>a</sup>See Ref. 13.

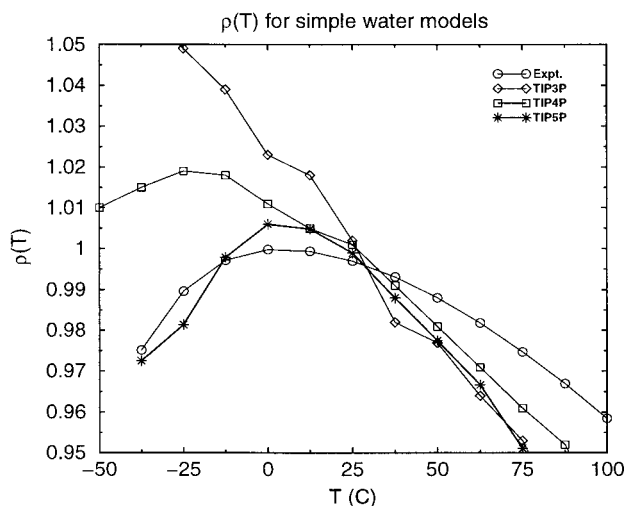


FIG. 2. Density of TIP $n$ P water models vs experiment as a function of temperature at 1 atm.

the results for TIP3P and TIP4P, while the isothermal compressibility  $\kappa$  shows improved accord with experiment, and  $\alpha$  is too high for all the models.

The results for the density as a function of temperature for the TIP5P model are presented in Fig. 2 along with the experimental data<sup>39</sup> and the prior results for the TIP3P and TIP4P models.<sup>13</sup> The density maximum for TIP5P water is correctly located at the experimental value of 4 °C within the statistical noise of the calculations. The results at the high temperatures are well converged and show that the density decreases too rapidly as the temperature increases. This yields the overestimates of  $\alpha$  at 25 °C and a displacement of the critical temperature to too low values. This is a general feature of the three- to five-site models; however, the existence of a TMD and the density profile in its vicinity are strikingly improved by increasing the number of interaction sites. The results at the temperatures below 0 °C also indicate a somewhat too steep decline in the density of TIP5P water with decreasing temperature. Thus, the computed density maximum is sharper than in real water, as also found for the ST2 model.<sup>6,12</sup> However, the average error in the density over the 100° temperature range from -37.5 to 62.5 °C of only 0.006 g cm<sup>-3</sup> with the TIP5P model represents a substantial improvement over all other water models.<sup>13</sup>

Table IV presents the thermodynamic properties for TIP5P as a function of temperature. The experimental energy is well reproduced over the range -25 to 62.5 °C, being somewhat too large in magnitude at low temperatures and too low in magnitude at high temperatures. The computed heats of vaporization decrease from 11.8 kcal/mol at -25 °C to 9.7 kcal/mol at 62.5 °C, while the experimental values decline from 11.0 to 10.1 kcal/mol over this range.<sup>10,13</sup> The results for  $C_p$  and  $\alpha$  were computed from the centered difference formula for estimating derivatives, except at the lowest and highest temperature reported where they were computed from the right and left difference formulas, respectively. Results from the fluctuation formulas were less well converged and are not presented. The computed  $C_p$  val-

TABLE IV. Thermodynamic properties for TIP5P water at 1 atm.<sup>a</sup>

$T$ (°C)	$-E$	$\rho$	$C_p$	$10^6 \kappa$	$10^5 \alpha$
-37.5	11.616±0.003	0.9725±0.0003			
-25.0	11.330±0.007	0.9814±0.0004	43.0±0.2	17±1	-125± 1
-12.5	10.849±0.008	0.9979±0.0008	39.4±0.3	24±1	-105± 3
0.0	10.498±0.008	1.0069±0.0010	33.8±0.5	31±1	-32± 5
12.5	10.168±0.007	1.0049±0.0011	30.9±0.8	36±1	33± 7
25.0	9.867±0.006	0.9991±0.0014	29.1±0.8	41±2	63± 6
37.5	9.590±0.006	0.9892±0.0012	27.6±0.3	47±1	87± 5
50.0	9.325±0.006	0.9775±0.0015	26.5±1.0	56±4	92±11
62.5	9.077±0.006	0.9667±0.0015	25.9±0.9	59±3	110±10
75.0	8.827±0.007	0.9512±0.0009	25.9±0.8	65±3	127± 7

<sup>a</sup>See Table III for units.

ues increase significantly as the temperature drops into the supercooled regime, in accord with experiment,<sup>9</sup> though the magnitudes are too high, and the anomalous constancy of the experimental  $C_p$  at 18 cal/mol-deg from 0 to 100 °C is not reproduced. Consistent with the  $\rho(T)$  curve in Fig. 2,  $\alpha$  decreases, passes through zero at the TMD, and becomes significantly negative as the temperature is decreased, also in accord with experiment.<sup>39</sup> The results for  $\kappa$  show trends similar to those reported for TIP3P and TIP4P water,<sup>13</sup> but are not well converged since they were computed from the fluctuation formula. The trend toward increasing  $\kappa$  with increasing temperature is reproduced, though the observed minimum for  $\kappa$  at 46 °C ( $44.8 \times 10^{-6}$  atm<sup>-1</sup>)<sup>8</sup> is not apparent in the computed results.

Results for the dielectric constant of TIP5P water over the temperature range from 0 to 100 °C at 1 atm pressure are presented in Table V and Fig. 3, accompanied by the experimental results.<sup>40</sup> The computed dielectric constant of 81.5 ± 1.6 at 25 °C agrees well with the experimental value of 78.3, and shows improvement over results of ~50–70 for the SPC, TIP3P, and TIP4P models.<sup>13</sup> The computed results in Fig. 3 nicely parallel the experimental data, so the slope  $d\epsilon/dT$  is correct near -0.32 deg<sup>-1</sup>. It has been suggested that a better description of the quadrupole moment is an important factor for improved reproduction of the dielectric constant.<sup>41(a)-(c)</sup> Table VI presents the values for the dipole and quadrupole moments for the TIP5P model in comparison with experiment and the TIP3P and TIP4P models. The units and coordinate system are as given in Ref. 41(d) and the calculation of the quadrupole moments used the center of mass of the molecule as the origin. The observed quadrupole moment is best reproduced by the TIP4P model, which also has the lowest dipole moment of the TIP $n$ P series. TIP5P has a quadrupole moment with mostly smaller components in

TABLE V. Computed and experimental dielectric constants at 1 atm.

$T$ (°C)	TIP5P	Expt. <sup>a</sup>
0.0	91.8±1.5	87.74
25.0	81.5±1.6	78.30
50.0	74.7±1.9	69.91
75.0	68.6±1.8	62.43
100.0	60.3±1.8	55.72

<sup>a</sup>Reference 40.

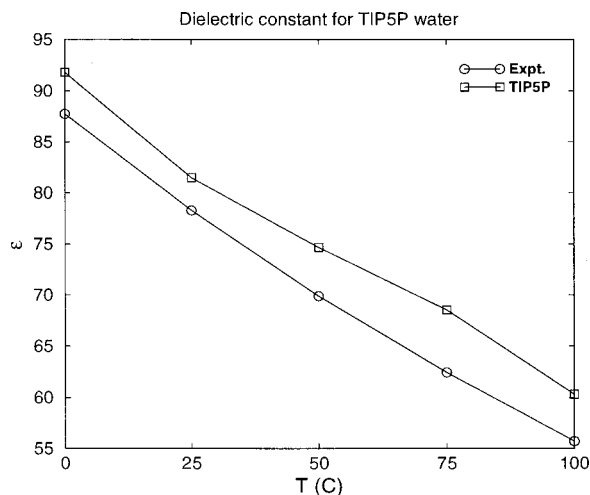


FIG. 3. Dielectric constant of TIP5P water vs experiment as a function of temperature at 1 atm.

magnitude and a larger dipole moment than TIP4P, but it is superior in reproducing the dielectric constant. The dielectric properties are undoubtedly affected by both the charge distribution and Lennard-Jones parameters.

## V. TEMPERATURE DEPENDENCE OF WATER STRUCTURE AND ENERGY DISTRIBUTIONS

Figures 4–6 present the oxygen–oxygen, oxygen–hydrogen, and hydrogen–hydrogen radial distribution functions at 25 °C and 1 atm along with the experimental data.<sup>42</sup> Overall, the results for the TIP4P and TIP5P models are similar and show improved structure over three-site alternatives.<sup>13</sup> The location of the maximum for the first peak of the O–O radial distribution function (rdf) is shifted inward  $\sim 0.03$  Å from the TIP4P result to  $2.73 \pm 0.01$  Å with TIP5P, the shape of the second peak is improved, and the first peak of the H–H rdf is somewhat too high. The latter feature was noted previously with the five-site ST2 and ST4 models<sup>41(c)</sup>; it is likely due to overly stiff angle bending in the potential energy surface for the dimer, as presented in Sec. VII. The temperature dependence of the radial distribution functions is illustrated in Figs. 7–9. The expected reduction in structure with increasing temperature is observed. The separation of nearest and second-nearest neighbors becomes much sharper in the OO rdf at  $-25$  °C, which is consistent with adoption of a more ice-I-like structure. This is discussed further below along with the effects of pressure on the liquid's structure.

TABLE VI. Dipole<sup>a</sup> and quadrupole<sup>b</sup> moments for the water monomer.

	$\mu$	$Q_{xx}$	$Q_{yy}$	$Q_{zz}$
Expt. <sup>c</sup>	1.85	2.63	-2.50	-0.13
TIP3P	2.35	1.76	-1.68	-0.08
TIP4P	2.18	2.20	-2.09	-0.11
TIP5P	2.29	1.65	-1.48	-0.17

<sup>a</sup>Units are  $10^{-18}$  esu-cm.

<sup>b</sup>Units are  $10^{-26}$  esu-cm<sup>2</sup>.

<sup>c</sup>References 41(d) and 41(e).

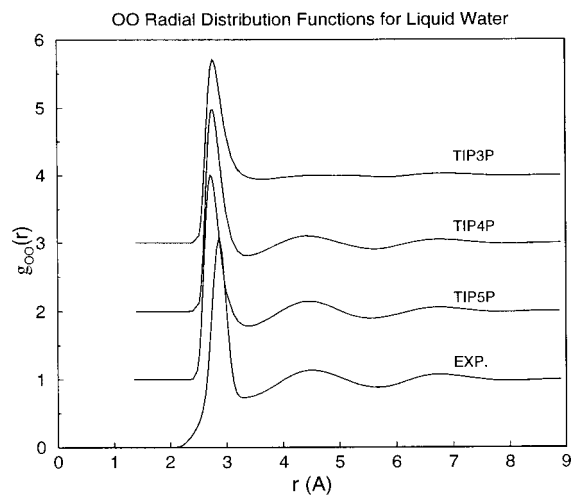


FIG. 4. OO radial distribution functions for water at 25 °C and 1 atm.

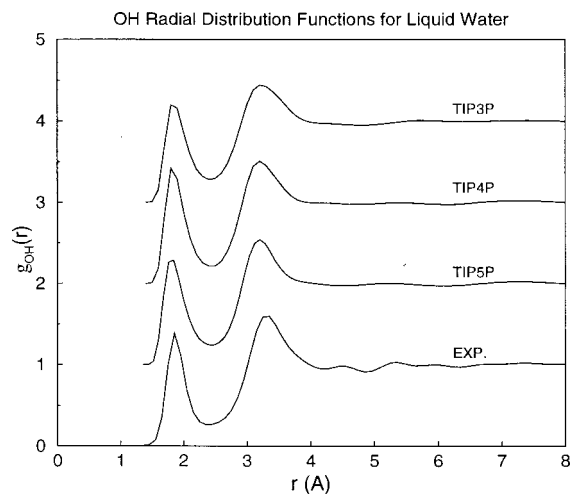


FIG. 5. OH radial distribution functions for water at 25 °C and 1 atm.

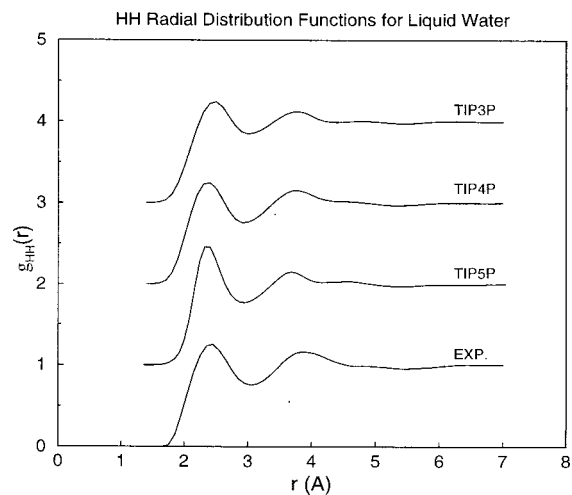


FIG. 6. HH radial distribution functions for water at 25 °C and 1 atm.

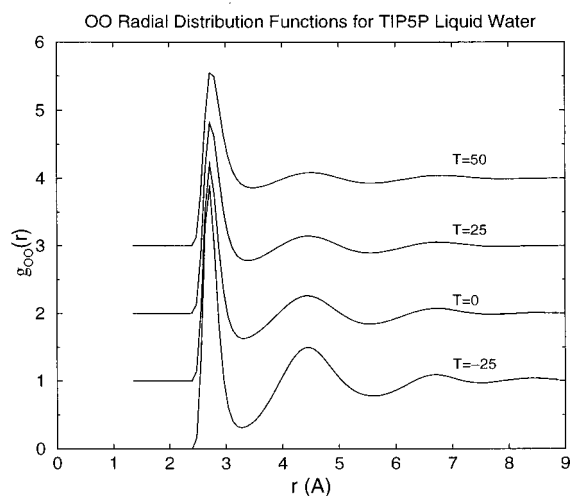


FIG. 7. Temperature dependence of the OO radial distribution function for TIP5P water at 1 atm.

The distributions of total intermolecular interaction energies for monomers in the liquid and the distributions of individual water–water interaction energies (the energy pair distributions) are presented in Figs. 10 and 11 as a function of temperature. These distributions exhibit an increased population of lower-energy configurations and narrower widths as the temperature decreases. The energy pair distributions indicate that as the temperature is decreased there is again a cleaner separation between hydrogen-bonded nearest neighbors and the more distant molecules. The minimum near  $-2.3$  kcal/mol becomes more distinct; integration to this point yields estimates for the average number of hydrogen bonds per water molecule of 3.9, 3.8, 3.7, and 3.6 at  $-25$ , 0, 25, and  $50$  °C. Thus, although the hydrogen bonding remains basically tetrahedral, a wider range of geometries and energies are explored with increasing temperature. The present results are very similar to those for TIP4P water, which have been discussed at length.<sup>3</sup>

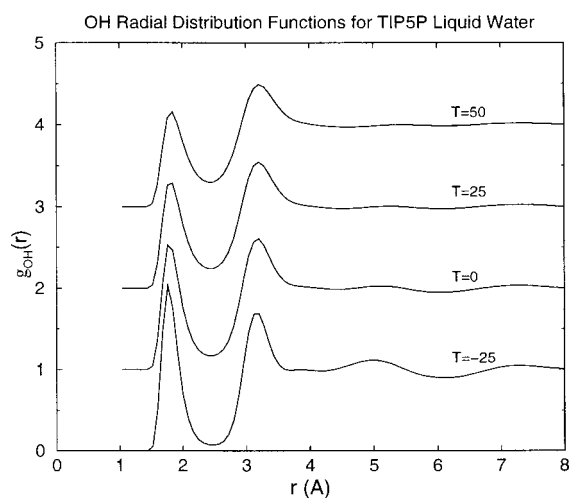


FIG. 8. Temperature dependence of the OH radial distribution function for TIP5P water at 1 atm.

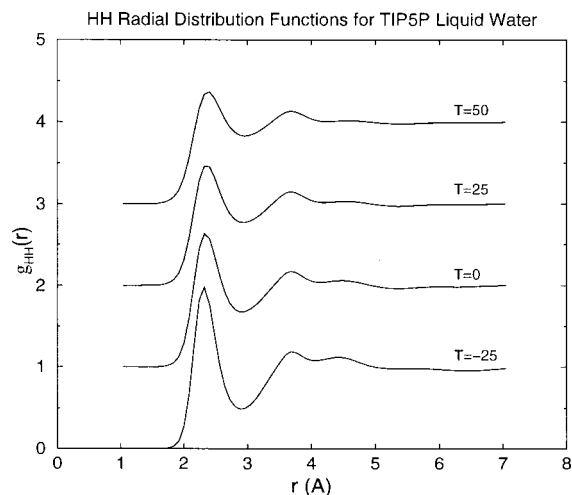


FIG. 9. Temperature dependence of the HH radial distribution function for TIP5P water at 1 atm.

## VI. PRESSURE DEPENDENCE OF THERMODYNAMIC AND STRUCTURAL PROPERTIES

There has been much investigation of the behavior of water as a function of pressure,<sup>9(a),9(b),39,43–50</sup> and on the similarities and differences in the dependencies on pressure and temperature.<sup>43</sup> The properties of TIP5P water were examined at a range of higher pressures by performing the calculations detailed in Table II(b). A pressure scan was carried out at  $25$  °C, and temperature scans were performed at 1000 and 2000 atm. It was found that at a fixed temperature, increasing the pressure did not lead to the convergence difficulties that were caused by decreasing the temperature at a fixed pressure. This allowed the high-pressure calculations at  $25$  °C to be comparatively short. In Tables VII(a) and VII(b), the thermodynamic properties for the TIP5P model at a variety of high-pressure state points are presented. The energy decreases slightly as the pressure is increased, in agreement with results for TIP4P water<sup>49</sup> and experimental data.<sup>44</sup> The computed variation of the density at  $25$  °C from 1 to 10 000

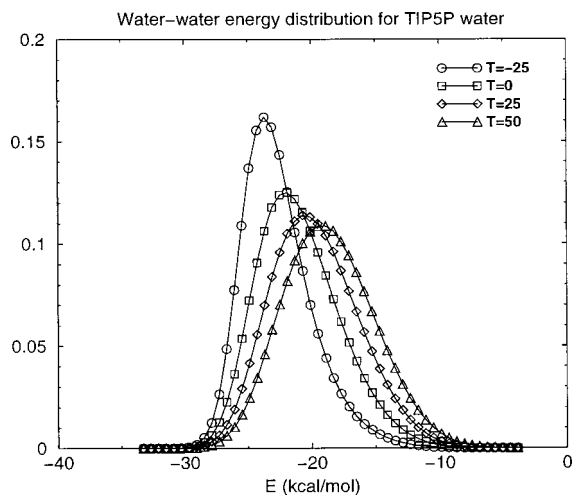


FIG. 10. Distributions of the total intermolecular binding energy for monomers in liquid TIP5P water at 1 atm. Units for the ordinate are mol fraction per kcal/mol.

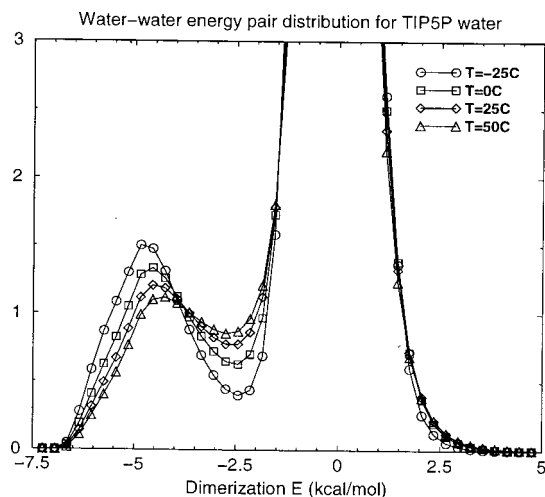


FIG. 11. Distributions of individual water-water interaction energies for TIP5P water at 1 atm. Units for the ordinate are number of molecules per kcal/mol.

atm ( $\sim 0.1013$  to  $1013$  MPa) is compared with the experimental data in Fig. 12. The results for TIP5P water below  $1000$  atm agree well with experiment and confirm that the model's isothermal compressibility  $\kappa$  at  $25^\circ\text{C}$  and  $1$  atm is reasonable (Table III). At higher pressures, TIP5P is somewhat more compressible than real water, with the error increasing to  $\sim 3\%$  at  $9000$  atm. If there is an implication for the repulsive part of the Lennard-Jones 12-6 potential from

TABLE VII. (a) Thermodynamic properties for TIP5P water at  $25^\circ\text{C}$  and elevated pressures.<sup>a</sup> (b) Energy and density for TIP5P water at elevated pressures and at a range of temperatures.

(a)					
$P$ (atm)	$-E$	$\rho$	$C_p$	$\kappa$	$\alpha$
1	$9.867 \pm 0.006$	$0.9991 \pm 0.0014$	$24.9 \pm 0.8$	$41 \pm 2$	$72 \pm 6$
1000	$9.929 \pm 0.005$	$1.0528 \pm 0.0007$	$25.8 \pm 3.3$	$32 \pm 3$	$67 \pm 18$
2000	$9.968 \pm 0.004$	$1.0922 \pm 0.0007$	$22.7 \pm 2.2$	$36 \pm 6$	$23 \pm 30$
3000	$9.994 \pm 0.015$	$1.1276 \pm 0.0009$	$21.0 \pm 1.0$	$21 \pm 1$	$56 \pm 11$
4000	$10.040 \pm 0.012$	$1.1591 \pm 0.0011$	$22.9 \pm 1.8$	$20 \pm 1$	$36 \pm 12$
5000	$10.078 \pm 0.001$	$1.1828 \pm 0.0011$	$25.2 \pm 1.6$	$17 \pm 1$	$67 \pm 11$
6000	$10.060 \pm 0.015$	$1.2051 \pm 0.0009$	$21.1 \pm 1.4$	$19 \pm 2$	$65 \pm 14$
8000	$10.105 \pm 0.013$	$1.2453 \pm 0.0016$	$19.8 \pm 0.9$	$13 \pm 1$	$49 \pm 9$
10000	$10.156 \pm 0.010$	$1.2830 \pm 0.0007$	$20.3 \pm 1.1$	$12 \pm 1$	$50 \pm 10$

(b)			
$T$ ( $^\circ\text{C}$ )	$P$ (atm)	$-E$ (kcal/mol)	$\rho$ ( $\text{g}/\text{cm}^3$ )
-25.0	1000	$11.144 \pm 0.002$	$1.0362 \pm 0.0004$
-12.5	1000	$10.757 \pm 0.002$	$1.0532 \pm 0.0005$
0.0	1000	$10.463 \pm 0.003$	$1.0590 \pm 0.0005$
12.5	1000	$10.184 \pm 0.003$	$1.0553 \pm 0.0005$
25.0	1000	$9.929 \pm 0.005$	$1.0528 \pm 0.0007$
-37.5	2000	$11.294 \pm 0.002$	$1.0936 \pm 0.0003$
-25.0	2000	$11.009 \pm 0.002$	$1.1027 \pm 0.0004$
-12.5	2000	$10.725 \pm 0.003$	$1.1095 \pm 0.0004$
0.0	2000	$10.460 \pm 0.003$	$1.1029 \pm 0.0005$
12.5	2000	$10.195 \pm 0.003$	$1.1003 \pm 0.0005$
25.0	2000	$9.968 \pm 0.004$	$1.0922 \pm 0.0007$

<sup>a</sup>See Table III for units.

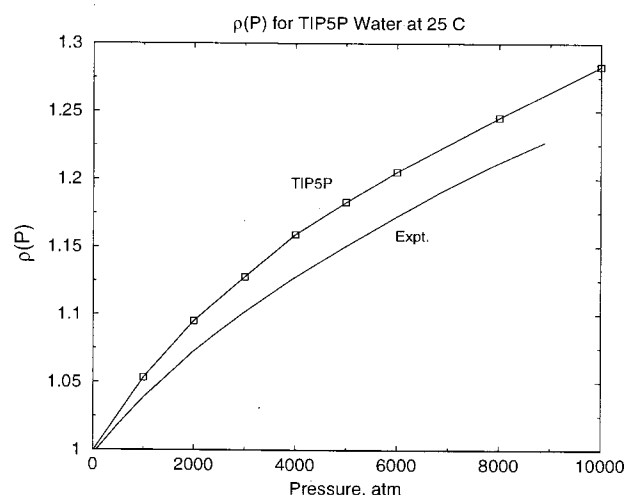


FIG. 12. Density of TIP5P water vs experiment as a function of pressure at  $25^\circ\text{C}$ .

these results, it would be that it is a little too soft at short range. However, the electrostatics also undoubtedly influence  $(dp/dP)_T$ .

The energy distributions at the elevated pressures are not presented. Shifts were obtained in agreement with results previously reported.<sup>47,49</sup> The shifts are much less than those from the temperature changes in Figs. 10 and 11. The effect of pressure on the OO rdf at  $25^\circ\text{C}$  is illustrated in Fig. 13. If the normalization of the rdf by division by the average density is removed, then the scaled plots in Fig. 14 are obtained. The latter figure shows that, in fact, there is not density loss in the vicinity of the second peak near  $4.5$  Å, but rather that the overall density increase at higher pressures particularly features enhanced density of water molecules at OO separations near  $3.3$  and  $6$  Å. Though the second neighbors are at  $4.5$  Å in ice I, it is well known that ices II, III, and V, which have densities near  $1.2$   $\text{g}/\text{cm}^3$ , have non-hydrogen-bonded neighbors at OO separations of  $3.2$ – $3.5$  Å.<sup>50</sup> Similar penetration of hydrogen-bonded networks in the liquid at such densities is reasonable.

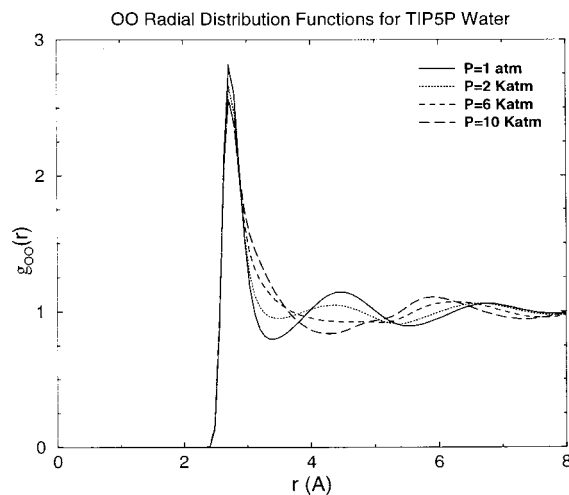


FIG. 13. Pressure dependence of OO radial distribution function for TIP5P water at  $25^\circ\text{C}$ .

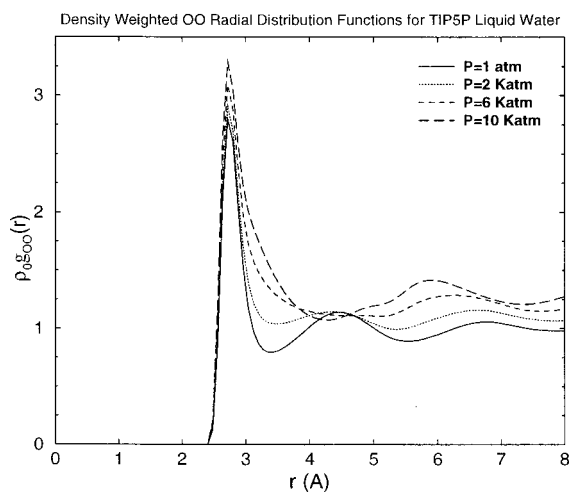


FIG. 14. Pressure dependence of density-weighted OO radial distribution function for TIP5P water at 25 °C.

The results for the energy and density from the temperature scans at 1000 and 2000 atm are presented in Table VII(b). In addition, the density versus temperature curves for TIP5P water at 1, 1000, and 2000 atm are plotted in Fig. 15 along with the experimental data.<sup>39,44</sup> The computations correctly reflect that the temperature of maximum density shifts to lower temperature as the pressure is increased. At higher pressures, the maximum in the experimental profile is lost, although this phenomenon is coupled with the unusual behavior of water at very low temperatures.<sup>9b</sup> Further exploration of TIP5P water in the supercooled region at elevated pressures is desirable,<sup>12</sup> although very long runs will be required to achieve well-converged results.

## VII. PROPERTIES OF THE TIP5P WATER DIMER

It has been noted that the common failure of potential functions in reproducing the TMD may be related to inadequacies in their description of the energy of the dimer as a function of the tilt angle  $\tau$  in Fig. 16.<sup>13,51</sup> The water dimer

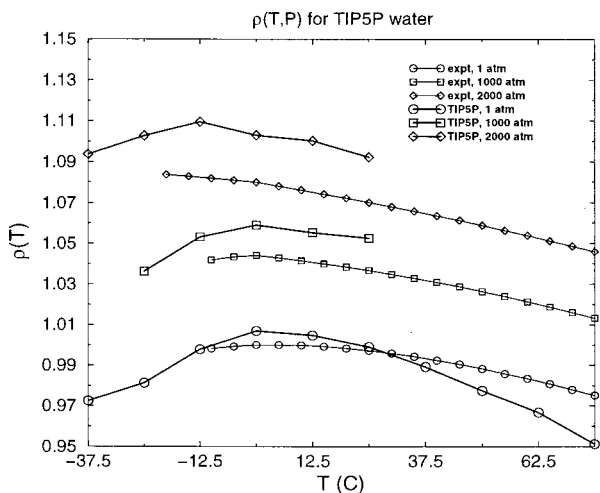


FIG. 15. Temperature dependence of the density of TIP5P water vs experiment at three pressures.

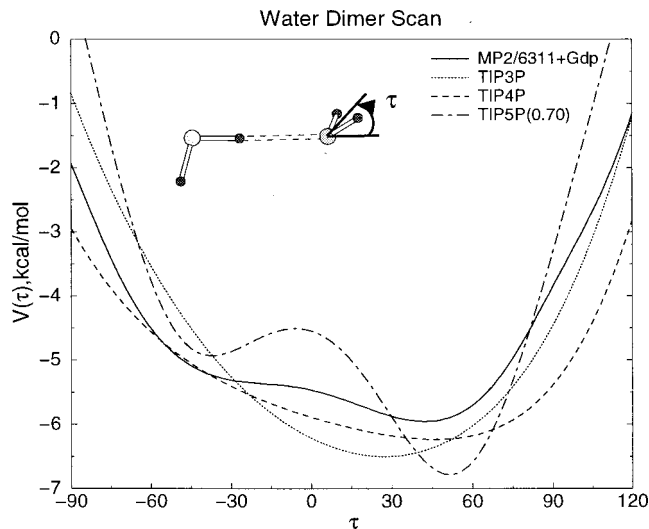


FIG. 16. Computed energy of the water dimer as a function of the flap angle  $\tau$ .

system has been studied extensively and the global minimum for the water dimer has been established to occur with a roughly linear hydrogen bond and with  $\tau$  near 57°.<sup>52–58</sup> Results of geometry optimizations for the linear water dimer using the TIPnP models are summarized in Table VIII. Effective pair potentials for liquid water feature optimal OO separations for the water dimer that are too short by about 0.3 Å and dimerization energies that are too high by about 1 kcal/mol.<sup>1–6</sup> These differences compensate for the primitive description of the electrostatics. Such models are not intended for use for gaseous water or the liquid at low densities. Improvement to have a model that works well at both high and low densities requires a more sophisticated charge distribution and/or explicit polarization.

The results of energy scans versus  $\tau$  for the linear dimer using rigid monomers are presented in Fig. 16. The force-field calculations were performed with the BOSS program<sup>36</sup> and the quantum mechanical calculations were carried out with GAUSSIAN 95.<sup>59</sup> The latter calculations involved a geometry optimization for the six intermolecular variables at the MP2/6-311+G(d,p) level, followed by an energy scan for  $\tau$  at the same level with the OO distance fixed at the optimal value. Analogous calculations were performed with the TIPnP models. The *ab initio* calculations yielded a minimum for the dimer with  $r_{OO}=2.92$  Å,  $\tau=42^\circ$  and a dimerization energy,  $\Delta E$ , of  $-5.96$  kcal/mol. The energy curve is significantly narrower with the TIP3P model, which also has the minimum shifted to  $\tau=27^\circ$ . The profile is better reproduced

TABLE VIII. Optimized geometry and dimerization energy for the linear water dimer.

	TIP3P	TIP4P	TIP5P	Expt. <sup>a</sup>
$r(OO)$ , Å	2.74	2.75	2.68	$2.98 \pm 0.02$
$\tau$ , deg	27	46	51	$57 \pm 10$
$-\Delta E$ , kcal/mol	6.50	6.24	6.78	$5.4 \pm 0.5$

<sup>a</sup>Reference 58 for  $(D_2O)_2$ .

TABLE IX. Five-point models examined to reproduce  $\rho(T)$  for liquid water.<sup>a</sup>

	TIP5P(0.4875)	TIP5P(0.60)	TIP5P(0.65)	TIP5P(0.70)
$\sigma_0$ (Å)	3.140	3.145	3.133	3.120
$\epsilon_0$ (kcal/mol)	0.16	0.16	0.16	0.16
$r_{OL}$ (Å)	0.4875	0.60	0.65	0.70
$q_L(e)$	-0.290	-0.266	-0.254	-0.241

<sup>a</sup>In all cases,  $r_{OH}=0.9572$  Å,  $\theta_{HOH}=104.52^\circ$ , and  $\theta_{LOL}=109.47^\circ$ .

with TIP4P, which has its minimum near  $\tau=46^\circ$ . Both the *ab initio* results and the TIP4P model have a broad region for  $\tau$  between  $\pm 60^\circ$  in which the energy remains less than 1 kcal/mol above the minimum. Using the TIP5P model the energy profile is overly structured, with a deeper well in the more favorable tetrahedral position near  $\tau\approx+50^\circ$  and a less deep well near the other tetrahedral position at  $\tau\approx-40^\circ$ . The favoring of tetrahedral orientations for five-site water models has been noticed previously<sup>51</sup> and is related to the placement of the partial negative charges in the lone-pair positions. Clearly, as the lone-pair sites are contracted toward the oxygen, the TIP5P curve would collapse toward the TIP3P one.

Figure 16 demonstrates that the dimer surface as a function of  $\tau$  is closer to the *ab initio* results with the TIP4P model than with TIP5P; however, it is also clear that TIP5P is overall the better model for liquid water and certainly yields the better density profile (Fig. 2). This is not inconsistent, if polarization in the condensed phase leads on average to an effective two-body potential that more sharply favors the tetrahedral disposition of hydrogen bonds.

### VIII. REPRODUCING THE DENSITY MAXIMUM AND SIZE DEPENDENCE OF THE RESULTS

As stated above, the goal was to develop the simplest potential function, which reproduces well the density anomaly of liquid water, while simultaneously yielding good thermodynamic and structural properties near 25 °C and 1 atm. Additional studies of three- and four-site models, including the introduction of internal flexibility and replacement of the 12-6 Lennard-Jones form, did not yield improvement for the density profiles over TIP4P. Five-site models were then explored with  $\sigma$  and  $\epsilon$  near the TIP3P and TIP4P values and with the L1-O-L2 angle constrained to be 109.47°. A primary focus became establishing the influence of the distance between the oxygen and the negatively charged sites,  $r_{OL}$ , on the density profiles. Once this was optimized, adjustments could be made to fine-tune the charge and Lennard-Jones parameters.

Series of calculations were performed over a range of temperatures for four alternative models using a more computationally tractable box size of 216 molecules. The parameters for the models are listed in Table IX. TIP5P(0.60) has  $r_{OL}=0.60$  Å and was developed<sup>27</sup> by varying the  $r_{OL}$  distance and charges to get a dipole moment of approximately 2.2 D for the monomer, a dimerization energy of between -6.0 and -6.5 kcal/mol, and correct values for the energy and density of the liquid at 25 °C and 1 atm. Note that the model ultimately developed has a dimerization energy out-

TABLE X. Lengths<sup>a</sup> of equilibration/averaging periods for Monte Carlo simulations with 216 molecules for five-point models of water at 1 atm.

T (°C)	TIP5P(0.4875)	TIP5P(0.60)	TIP5P(0.65)	TIP5P(0.70)
-50.0	100/600			
-37.5	100/450	100/450		
-25.0	100/300	100/300	100/300	
-12.5	75/225	75/225	75/225	100/300
0.0	75/175	75/175	75/175	100/300
12.5	50/150	50/150	50/175	50/250
25.0	25/125	25/125	50/100	50/150
37.5	25/75	25/75	25/75	25/75
50.0	25/75	25/75	25/75	25/75

<sup>a</sup>Millions of MC steps.

side this range. For TIP5P(0.4875), the negative charges were moved toward the oxygen by 0.1125 Å and the charge was modified to reproduce the energy and density. Based on the shift in the  $\rho(T)$  curves for these two models, TIP5P(0.65) was developed by increasing the distance between the lone-pair interaction site and the oxygen atom and by modifying the Lennard-Jones  $\sigma$  parameter and the charge, again to reproduce the liquid's energy and density at 25 °C. Further refinement yielded TIP5P(0.70), which is TIP5P, through increasing the  $r_{OL}$  distance to 0.70 Å and modifying the other parameters. Scans for the dimerization energy as a function of  $\tau$  were performed and showed the expected strengthening of the double well form in Fig. 16 with increasing  $r_{OL}$ .

Monte Carlo simulations for the liquid with each of these models were executed to establish the effect of varying the  $r_{OL}$  distance on the calculated properties. The lengths of the equilibration and averaging stages for these calculations are listed in Table X. The calculations were similar to those already described except that the box size was 216 molecules and the intermolecular nonbonded cutoff distance was 8.0 Å. The results for the density and energy are recorded in Tables XI and Table XII. The small dependence of the energy and density on the number of molecules for fixed-charge models has been noted before.<sup>3,60</sup> The same is found for TIP5P(0.70) water; runs with 216 (Tables XI and XII), 267, and 512 (Table IV) molecules and cutoffs of 8.0, 8.5, and 9.0 Å, respectively, show an increase of 1% for both the energy and the density at 25 °C and 1 atm. Calculations have also been performed for 267 molecules with a cutoff of 8.5 Å and use of a reaction field for long-range interactions<sup>35(b)</sup>; the same trend is found with  $\sim 1\%$  increases in the energy and density. What has not been noted before is the dependence of the temperature of maximum density on the system size. The results in Tables IV and XI indicate that upon decreasing the number of molecules, the density maximum of TIP5P(0.70) is increased by 5–10 °C. Results not presented indicate that a similar shift exists for TIP5P(0.65), which has a temperature of maximum density close to the experimental value for a box of 216 molecules, but whose maximum decreases  $\sim 10$  °C upon increasing the number of molecules to 512.

It was found that for a given  $r_{OL}$  distance, the energy and density at 25 °C could be reproduced by simultaneously varying the partial charges and the Lennard-Jones  $\sigma$ . Results not presented indicate that the shapes of the curves, i.e., the

TABLE XI. Density ( $\text{g}/\text{cm}^3$ ) for five-point models of water with 216 molecules at 1 atm.

$T$ ( $^{\circ}\text{C}$ )	TIP5P(0.4875)	TIP5P(0.60)	TIP5P(0.65)	TIP5P(0.70)
-50.0	$1.0246 \pm 0.0006$			
-37.5	$1.0256 \pm 0.0007$	$0.9724 \pm 0.0006$		
-25.0	$1.0242 \pm 0.0008$	$0.9896 \pm 0.0008$	$0.9722 \pm 0.0007$	
-12.5	$1.0200 \pm 0.0007$	$0.9971 \pm 0.0008$	$0.9896 \pm 0.0009$	$0.9749 \pm 0.0005$
0.0	$1.0139 \pm 0.0008$	$0.9956 \pm 0.0010$	$0.9973 \pm 0.0011$	$0.9852 \pm 0.0010$
12.5	$1.0050 \pm 0.0010$	$0.9899 \pm 0.0008$	$0.9909 \pm 0.0008$	$0.9925 \pm 0.0009$
25.0	$0.9969 \pm 0.0008$	$0.9806 \pm 0.0010$	$0.9880 \pm 0.0010$	$0.9886 \pm 0.0011$
37.5	$0.9869 \pm 0.0013$	$0.9728 \pm 0.0011$	$0.9779 \pm 0.0011$	$0.9840 \pm 0.0012$
50.0	$0.9723 \pm 0.0012$	$0.9609 \pm 0.0012$	$0.9702 \pm 0.0011$	$0.9750 \pm 0.0011$

temperature at which the maximum occurs and the difference between, e.g., the density at the maximum and the density at  $25^{\circ}\text{C}$ , are similar for models with identical  $r_{\text{OL}}$  distances and minor changes in the other parameters. Thus, in Fig. 17, the density is plotted as a function of temperature for four models with varying  $r_{\text{OL}}$ . Note that the curves in Fig. 17 have each been offset along the ordinate in order to have each a common density at  $25^{\circ}\text{C}$ . The effect of varying  $r_{\text{OL}}$  is then seen more clearly.

All four models yield a density maximum, although its position and the density at the TMD vary widely. The tetrahedral charge distribution captures an important aspect of the intermolecular energetics required to model well the density variations as a function of temperature. While the qualitative feature of a density maximum is clearly obtained for models with  $r_{\text{OL}}$  greater than  $\sim 0.5 \text{ \AA}$ , the exact positioning of the lone-pair sites is important for its quantitative reproduction. With an  $r_{\text{OL}}$  of  $0.6 \text{ \AA}$ , the density maximum occurs between  $-15$  and  $-25^{\circ}\text{C}$ , while moving the lone-pair sites toward the oxygen by only  $0.1125 \text{ \AA}$  to an  $r_{\text{OL}}$  of  $0.4875 \text{ \AA}$  significantly degrades the density profile. Diminution of  $r_{\text{OL}}$  to zero, while modifying the charge to reproduce the energy and density and while keeping the Lennard-Jones parameters approximately fixed, produces the TIP3P model. Its  $\rho(T)$  curve in Fig. 2 monotonically increases as the temperature is decreased.

Thus, the anisotropy introduced in the potential function with the lone-pair sites is rapidly lost for  $r_{\text{OL}}$  below  $0.6 \text{ \AA}$ . On the other hand, increasing  $r_{\text{OL}}$  much beyond this point pushes the TMD to too high a temperature. The pattern continues with the ST2 model<sup>6,12</sup>; though the scaling of the electrostatics at short range complicates the analysis, it has the lone-pair sites at a still greater distance ( $r_{\text{OL}}=0.8 \text{ \AA}$ ) and its

TMD occurs at significantly higher temperature,  $30\text{--}40^{\circ}\text{C}$ , than for the five-site models examined here. Besides moving the TMD to higher temperature, increasing  $r_{\text{OL}}$  is also found to move the density at the TMD to lower values, given that the value of the density at some state point, e.g.,  $25^{\circ}\text{C}$ , is fixed. It appears that the charge distribution is the primary determinant of the shape of the  $\rho(T)$  curve. Further improvement in the computed results, e.g., at high temperature and pressure, would likely necessitate the use of a larger number of charged sites or explicit polarization as well as much effort at optimization of the model.

## IX. FURTHER DISCUSSION

The TIP5P model appears to yield improved results for  $\rho(T)$  and the TMD by forcing tetrahedral arrangements for hydrogen-bonded pairs to be more attractive than with real water. Though the computed radial distribution functions are in generally good accord with experiment, the enforced tetrahedrality is undoubtedly responsible for the first peak in the HH rdf being too high (Fig. 6). The overly tetrahedral description of the hydrogen bonding promotes the existence of a TMD at low temperature; however, the description of the interactions between less well-bound neighbors, which are more important at higher temperatures and pressures, may be adversely affected. Such less accurate treatment of non-hydrogen-bonded neighbors for all of the common fixed-charge models may be responsible for the density always rising too rapidly with increasing pressure or with decreasing temperature above the TMD. Another general problem is that the first peak in the OO rdf is always at too short a distance with the simple fixed-charge models. This discrep-

TABLE XII. Potential energy (kcal/mol) for five-point models of water with 216 molecules at 1 atm.

$T$ ( $^{\circ}\text{C}$ )	TIP5P(0.4875)	TIP5P(0.60)	TIP5P(0.65)	TIP5P(0.70)
-50.0	$-11.398 \pm 0.003$			
-37.5	$-11.160 \pm 0.003$	$-11.407 \pm 0.004$		
-25.0	$-10.885 \pm 0.005$	$-11.047 \pm 0.005$	$-11.356 \pm 0.003$	
-12.5	$-10.660 \pm 0.005$	$-10.680 \pm 0.005$	$-10.911 \pm 0.007$	$-11.134 \pm 0.006$
0.0	$-10.417 \pm 0.005$	$-10.418 \pm 0.006$	$-10.590 \pm 0.008$	$-10.730 \pm 0.009$
12.5	$-10.186 \pm 0.005$	$-10.152 \pm 0.006$	$-10.312 \pm 0.006$	$-10.311 \pm 0.008$
25.0	$-9.965 \pm 0.005$	$-9.900 \pm 0.006$	$-10.010 \pm 0.007$	$-10.003 \pm 0.009$
37.5	$-9.771 \pm 0.006$	$-9.671 \pm 0.008$	$-9.751 \pm 0.008$	$-9.688 \pm 0.010$
50.0	$-9.552 \pm 0.005$	$-9.423 \pm 0.007$	$-9.511 \pm 0.007$	$-9.410 \pm 0.009$

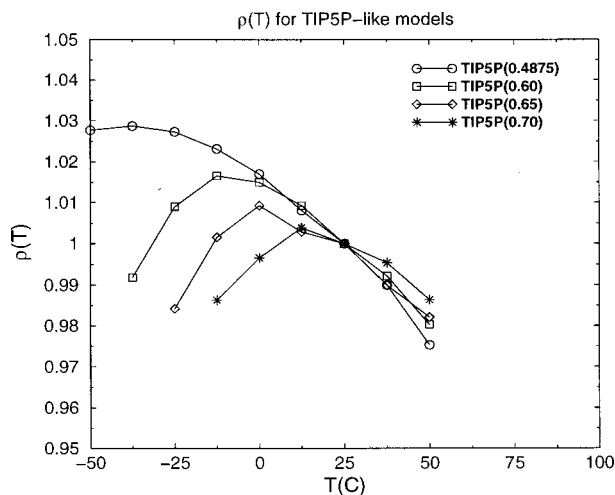


FIG. 17. Density of five-site water models as a function of temperature at 1 atm from MC simulations with 216 molecules. See Table XI for the exact numerical densities. In order to emphasize the effect that varying the oxygen to lone-pair interaction site distance has on the shape of the density profile, the results here have each curve offset along the ordinate to make the density at 25 °C equal to 1.0 g/cm<sup>3</sup>.

ancy can probably not be rectified without replacing the Lennard-Jones potential, introducing a scaling function, or adding explicit polarization or quantum effects.

Though structural changes were discussed above based on the radial distribution functions, some additional insights are notable from the isochoric temperature differentials for the oxygen–oxygen radial distribution function, as presented in Fig. 18. These have been measured<sup>61</sup> and effort has been directed at their interpretation.<sup>62,63</sup> Since *NPT* MC calculations were performed here, the pressures rather than the densities were fixed. Nevertheless, the densities at 12.5 and 0.0 °C were computed to be approximately identical at 1 atm. The same is true for the densities at 25 and –12.5 °C and also at 50 and –25 °C. Therefore, these pairs of temperatures were chosen to examine the rdf differences. It is seen that for

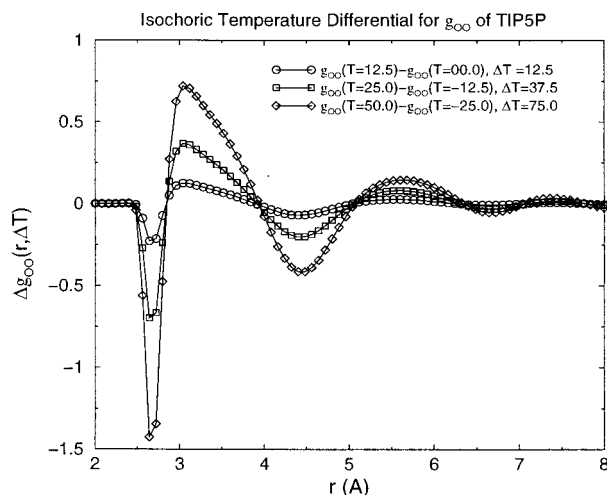


FIG. 18. Isochoric temperature differentials of the oxygen–oxygen radial distribution function for TIP5P water. Results are presented for three temperature differences at 1 atm.

the TIP5P model the magnitudes of the peaks and valleys, but not their positions, depend on the temperature difference, with isobestic points occurring at  $\sim 2.9, 3.9, 5.0,$  and  $6.3 \text{ \AA}$ . These locations agree well with the experimental values. There is reduced density in the first and second peaks of the OO rdf and filling-in on both sides of the second peak upon raising the temperature at constant density. It may also be noted that the magnitudes of the oscillations in the isochoric temperature differentials for TIP5P and real water are roughly linear in the temperature difference. These facts, and the correspondence of the extrema in Fig. 18 with oxygen–oxygen distances that are featured in ices I and II (or III), suggest two-state mixture models for the liquid.<sup>62,63</sup> In addition, nonisochoric pressure differentials can be computed from the results in Fig. 13. The results are quite similar to those calculated in Ref. 63 from the experimental data in Ref. 43(c), and which were used to further support a two-state model.<sup>63</sup>

Supercooled water has received much attention, often centering around the possible existence of a line of liquid–liquid phase transitions terminating at a second critical point.<sup>9(c),12,49,64–68</sup> The improved performance at low temperatures with the TIP5P model should aid such studies. However, it should be kept in mind that the TIP5P model has been optimized for use with 512 molecules, a spherical cut-off of 9.0 Å, and cubic periodic boundary conditions. If further calculations employ a different system size, the density maximum will be shifted somewhat, as noted above. In addition, while models such as TIP4P have often been used to calculate properties at state points far from their original realm of parameterization, caution is needed under such circumstances. The hydrogen bonding near optimal geometries seems to be reasonably well described, but less favorable interactions between near neighbors are more problematic with models in this class.

Related to the question of calculations on liquid water at low temperatures is the issue of the lengths of the averaging and equilibration periods needed to obtain converged results.<sup>13,14</sup> The requisite lengths for both periods increase significantly with decreasing temperature, while the dependence on increasing pressure was less severe. Thus, the calculations below 0 °C at 1 atm needed to be more than five times longer than the ones above 25 °C to achieve comparable convergence of the energy and density. Calculations of the present length and breadth would currently be very difficult to perform with a polarizable model. For example, the polarizable PPC model has been reported to have a density maximum near the experimental value based on molecular dynamics calculations, which consisted of 100 ps of equilibration and 300–500 ps of averaging.<sup>16</sup> A comparison between Monte Carlo and molecular dynamics for liquid hexane yielded an approximate equivalence between 10 ps of MD and 2000 MC passes. For a system with 500 molecules, this corresponds to a rough equivalence between 10<sup>7</sup> MC steps and 100 ps of MD.<sup>69</sup> Assuming a similar situation for water, the calculations for the PPC model correspond to  $\sim 10^7$  MC steps for equilibration and  $3\text{--}5 \times 10^7$  MC steps for averaging. For the present calculations below 0 °C and starting with a box equilibrated at a nearby temperature, the

equilibration stage took more than  $10^8$  configurations, and the averaging phase took substantially longer. At the low temperatures, there were occasional fluctuations along the Markov chain of  $\sim 1\%$  in the energy and density that lasted  $\sim 10^8$  steps. It was only after averaging  $\sim 10^9$  MC steps that it was possible to regard such segments as fluctuations. Since polarizable models require longer periods for equilibration and averaging than fixed-charge models,<sup>32,70</sup> it is unlikely that MD runs less than nanoseconds in length are sufficient to provide adequate enough precision for the densities at low temperature to establish decisively the density profile and TMD. This estimate is consistent with the analyses and run lengths of Baez and Clancy.<sup>14</sup>

## X. CONCLUSION

Classical Monte Carlo statistical mechanical simulations have been used to optimize a five-site, fixed-charge model of liquid water with emphasis on improving the computed density as a function of temperature and the position of the temperature of maximum density (TMD). Calculations in the *NPT* ensemble at 1 atm, in which the distance between the lone-pair sites and the oxygen,  $r_{OL}$ , varied between 0.4875 and 0.70 Å, demonstrated that a TMD can be achieved in this region of parameter space. In addition, as  $r_{OL}$  is increased, the TMD moves to higher temperature and the density at the maximum decreases toward the experimental value, if the models are parametrized to have the correct density at 25 °C. The final TIP5P model with an  $r_{OL}$  of 0.70 Å closely matches the experimental density and energy of liquid water at 25 °C and 1 atm. Furthermore, the density and energy as a function of temperature are reproduced with an average error of less than 1% from  $-37.5$  to  $62.5$  °C, the position of the TMD is correct, the dielectric constant at 25 °C is near 80 and shows the correct temperature dependence, the average error in the density as a function of pressure up to 9000 atm at 25 °C is less than 2%, the TMD shifts correctly to lower temperature with increasing pressure, and the radial distribution functions and their isochoric temperature differentials agree well with experiment. The principal problems are that the heat capacity is too high and the density increases too rapidly with increasing pressure or decreasing temperature above the TMD. The results for the water dimer overly favor tetrahedral geometries and show the usual underestimate of the OO distance for nonpolarizable water models. The latter differences are a consequence of accounting for multibody cooperative effects with a two-body effective potential.

Overall, the TIP5P model shows significant improvement in many areas over prior fixed-charge models for liquid water. It provides notably accurate results for the density from  $-37.5$  to  $62.5$  °C at 1 atm. Functional compatibility has been maintained with widely used force fields, and along with the excellent results for many properties, including the dielectric constant, the TIP5P model provides a basis for more accurate simulations of biomolecular systems. Additional studies of dynamical properties and aqueous solutions are being undertaken.

## ACKNOWLEDGMENTS

Gratitude is expressed to the National Science Foundation for support of this work. The authors are also grateful to Dr. Julian Tirado-Rives for helpful discussions and to Dr. Yu. E. Gorbaty and Dr. Liem X. Dang for data and unpublished results.

- <sup>1</sup>D. L. Beveridge, M. Mezei, P. K. Mehrotra, F. T. Marchese, G. Ravi-Shankar, T. Vasu, and S. Swaminathan, in *Molecular-Based Study of Fluids*, ACS Advances in Chemistry Series 204, edited by J. M. Haile and G. A. Mansoori (American Chemical Society, Washington, DC, 1983), p. 297.
- <sup>2</sup>W. L. Jorgensen, J. Chandrasekhar, J. D. Madura, R. W. Impey, and M. L. Klein, *J. Chem. Phys.* **79**, 926 (1983).
- <sup>3</sup>W. L. Jorgensen and J. D. Madura, *Mol. Phys.* **56**, 1381 (1985).
- <sup>4</sup>H. J. C. Berendsen, J. P. M. Postma, W. F. van Gunsteren, and J. Hermans, in *Intermolecular Forces*, edited by B. Pullman (Reidel, Dordrecht, 1981), p. 331.
- <sup>5</sup>H. J. C. Berendsen, J. R. Grigera, and T. P. Straatsma, *J. Phys. Chem.* **91**, 6269 (1987).
- <sup>6</sup>F. H. Stillinger and A. Rahman, *J. Chem. Phys.* **60**, 1545 (1974).
- <sup>7</sup>(a) A. A. Chialvo and P. T. Cummings, *J. Chem. Phys.* **101**, 4466 (1994); (b) G. Chalasiński, M. M. Szczesniak, P. Cieplak, and S. Scheiner, *ibid.* **94**, 2873 (1991); (c) S. Harrington, R. Zhang, P. H. Poole, F. Sciortino, and H. E. Stanley, *Phys. Rev. Lett.* **78**, 2409 (1997).
- <sup>8</sup>G. S. Kell, *J. Chem. Eng. Data* **20**, 97 (1975).
- <sup>9</sup>(a) C. A. Angell and H. Kanno, *Science* **193**, 1121 (1976); (b) H. Kanno and C. A. Angell, *J. Chem. Phys.* **73**, 1940 (1980); (c) C. A. Angell, M. Oguni, and W. J. Sichina, *J. Phys. Chem.* **86**, 998 (1982); (d) R. J. Speedy, *ibid.* **91**, 3354 (1987).
- <sup>10</sup>N. E. Dorsey, *Properties of Ordinary Water Substance* (Reinhold, New York, 1940).
- <sup>11</sup>(a) S. R. Billeter, P. M. King, and W. F. van Gunsteren, *J. Chem. Phys.* **100**, 6692 (1994); (b) C. H. Cho, S. Singh, and G. W. Robinson, *Phys. Rev. Lett.* **76**, 1651 (1996).
- <sup>12</sup>(a) P. H. Poole, F. Sciortino, U. Essman, and H. E. Stanley, *Nature (London)* **360**, 324 (1992); (b) *Phys. Rev. E* **48**, 3799 (1993); (c) **55**, 727 (1997).
- <sup>13</sup>W. L. Jorgensen and C. Jenson, *J. Comput. Chem.* **19**, 1179 (1998).
- <sup>14</sup>L. A. Baez and P. Clancy, *J. Chem. Phys.* **101**, 9837 (1994).
- <sup>15</sup>F. Sciortino and S. Sastry, *J. Chem. Phys.* **100**, 3881 (1994).
- <sup>16</sup>I. M. Svishchev, P. G. Kusalik, J. Wang, and R. J. Boyd, *J. Chem. Phys.* **105**, 4742 (1996).
- <sup>17</sup>A. Wallqvist and B. J. Berne, *J. Phys. Chem.* **97**, 13841 (1993).
- <sup>18</sup>A. Wallqvist and P. O. Astrand, *J. Chem. Phys.* **102**, 6559 (1995).
- <sup>19</sup>G. C. Lie and E. Clementi, *Phys. Rev. A* **33**, 2679 (1986).
- <sup>20</sup>A. Wallqvist, *Chem. Phys.* **148**, 439 (1990).
- <sup>21</sup>D. E. Smith and A. D. J. Haymet, *J. Chem. Phys.* **96**, 8450 (1992).
- <sup>22</sup>O. Teleman, B. Jonsson, and S. Engstrom, *Mol. Phys.* **60**, 193 (1987).
- <sup>23</sup>S. B. Zhu, S. Yao, J. B. Zhu, S. Singh, and G. W. Robinson, *J. Phys. Chem.* **95**, 6211 (1991).
- <sup>24</sup>S. B. Zhu, S. Singh, and G. W. Robinson, *J. Chem. Phys.* **95**, 2791 (1991).
- <sup>25</sup>D. J. Swanton, G. B. Bacskay, and N. S. Hush, *Chem. Phys.* **82**, 303 (1983).
- <sup>26</sup>D. J. Swanton, G. B. Bacskay, and N. S. Hush, *J. Chem. Phys.* **84**, 5715 (1986).
- <sup>27</sup>M. Richardson and W. L. Jorgensen, unpublished results.
- <sup>28</sup>M. Sprik and M. L. Klein, *J. Chem. Phys.* **89**, 7556 (1988).
- <sup>29</sup>J. Caldwell, L. X. Dang, and P. A. Kollman, *J. Am. Chem. Soc.* **112**, 9144 (1990).
- <sup>30</sup>T. P. Straatsma and J. A. McCammon, *Chem. Phys. Lett.* **177**, 433 (1991).
- <sup>31</sup>S. W. Rick, S. J. Stuart, and B. J. Berne, *J. Chem. Phys.* **101**, 6141 (1994).
- <sup>32</sup>M. W. Mahoney and W. L. Jorgensen (unpublished).
- <sup>33</sup>W. L. Jorgensen, *Chem. Phys. Lett.* **92**, 405 (1982).
- <sup>34</sup>W. L. Jorgensen, in *Encyclopedia of Computational Chemistry*, edited by P. v. R. Schleyer (Wiley, New York, 1998), p. 1754.
- <sup>35</sup>(a) H. E. Alper and R. M. Levy, *J. Chem. Phys.* **91**, 1242 (1989); (b) J. W. Essex and W. L. Jorgensen, *J. Phys. Chem.* **99**, 17956 (1995).
- <sup>36</sup>W. L. Jorgensen, BOSS, Version 3.8 Yale University, New Haven, CT, 1997.
- <sup>37</sup>(a) M. P. Allen and D. J. Tildesley, *Computer Simulation of Liquids* (Ox-

- ford University Press, Oxford, 1987); (b) D. Frenkel and B. Smit, *Understanding Molecular Simulation* (Academic, San Diego, 1996).
- <sup>38</sup>W. W. Wood, in *Physics of Simple Liquids*, edited by H. N. V. Temperley, J. S. Rowlinson, and G. S. Rushbrooke (North Holland, Amsterdam, 1968).
- <sup>39</sup>H. Sato, M. Uematsu, K. Watanabe, A. Saul, and W. Wagner, *J. Phys. Chem. Ref. Data* **17**, 1439 (1988).
- <sup>40</sup>C. G. Malmberg and A. A. Maryott, *J. Res. Natl. Bur. Stand.* **56**, 1 (1956).
- <sup>41</sup>(a) K. Watanabe and M. L. Klein, *Chem. Phys.* **131**, 157 (1989); (b) S. L. Carnie and G. N. Patey, *Mol. Phys.* **47**, 1129 (1982); (c) T. Head-Gordon and F. H. Stillinger, *J. Chem. Phys.* **98**, 3313 (1993); (d) J. Verhoeven and A. Dymanus, *ibid.* **52**, 3222 (1970); (e) S. A. Clough, Y. Beers, G. P. Klein, and L. S. Rothman, *ibid.* **59**, 2254 (1973).
- <sup>42</sup>(a) A. K. Soper and M. G. Phillips, *Chem. Phys.* **107**, 47 (1986); (b) A. K. Soper, **107**, 61 (1986); (c) *J. Chem. Phys.* **101**, 6888 (1994).
- <sup>43</sup>(a) Y. E. Gorbaty and Y. N. Demianets, *Chem. Phys. Lett.* **100**, 450 (1983); (b) Y. E. Gorbaty and Y. N. Demianets, *Mol. Phys.* **55**, 571 (1985); (c) A. V. Okhulkov, Y. N. Demianets, and Y. E. Gorbaty, *J. Chem. Phys.* **100**, 1578 (1994); (d) Y. E. Gorbaty, G. V. Bondarenko, A. G. Kalinichev, and A. V. Okhulkov, *Mol. Phys.* **96**, 1659 (1999).
- <sup>44</sup>(a) P. W. Bridgman, *Proc. Am. Acad. Arts Sci.* **48**, 309 (1912); (b) P. W. Bridgman, *J. Chem. Phys.* **5**, 964 (1937); (c) **3**, 597 (1935).
- <sup>45</sup>M. R. Reddy and M. Berkowitz, *J. Chem. Phys.* **87**, 6682 (1987).
- <sup>46</sup>R. W. Impey, M. L. Klein, and I. R. McDonald, *J. Chem. Phys.* **74**, 647 (1981); K. Bagchi, S. Balasubramanian, and M. L. Klein, *ibid.* **107**, 8561 (1997).
- <sup>47</sup>A. G. Kalinichev, Y. E. Gorbaty, and A. V. Okhulkov, *J. Mol. Liq.* **82**, 57 (1999).
- <sup>48</sup>H. Kanno and C. A. Angell, *J. Chem. Phys.* **70**, 4008 (1979).
- <sup>49</sup>J. D. Madura, B. M. Pettitt, and D. F. Calef, *Mol. Phys.* **64**, 325 (1988).
- <sup>50</sup>D. Eisenberg and W. Kauzmann, *The Structure and Properties of Water* (Oxford University Press, Oxford, 1969).
- <sup>51</sup>F. H. Stillinger, *J. Phys. Chem.* **74**, 3677 (1970).
- <sup>52</sup>K. S. Kim, B. J. Mhin, U. Choi, and K. Lee, *J. Phys. Chem.* **97**, 6649 (1992).
- <sup>53</sup>D. Feller, *J. Phys. Chem.* **96**, 6104 (1992).
- <sup>54</sup>S. Scheiner, *Annu. Rev. Phys. Chem.* **45**, 23 (1994).
- <sup>55</sup>B. J. Smith, D. J. Swanton, J. A. Pople, H. F. Schaefer, and L. Radom, *J. Chem. Phys.* **92**, 1240 (1990).
- <sup>56</sup>K. Kim and K. D. Jordan, *J. Phys. Chem.* **98**, 10089 (1994).
- <sup>57</sup>T. R. Dyke, K. M. Mack, and J. S. Muenter, *J. Chem. Phys.* **66**, 498 (1977).
- <sup>58</sup>R. S. Fellers, C. Leforestier, L. B. Braly, M. G. Brown, and R. J. Saykally, *Science* **284**, 945 (1999).
- <sup>59</sup>GAUSSIAN 95, Development Version (Revision E.1), M. J. Frisch, G. W. Trucks, H. B. Schlegel, G. E. Scuseria, M. A. Robb, J. R. Cheeseman, M. C. Strain, J. C. Burant, R. E. Stratman, G. A. Petersson, J. A. Montgomery, V. G. Zakrzewski, K. Raghavachari, P. Y. Ayala, Q. Cui, K. Morokuma, J. V. Ortiz, J. B. Foresman, J. Cioslowski, B. B. Stefanov, W. Chen, M. W. Wong, J. L. Andres, E. S. Replogle, R. Gomperts, R. L. Martin, D. J. Fox, T. Keith, M. A. Al-Laham, A. Nanayakkara, M. Challacombe, C. Y. Peng, J. P. Stewart, C. Gonzalez, M. Head-Gordon, P. M. W. Gill, B. G. Johnson, and J. A. Pople, Gaussian, Inc., Pittsburgh, PA, 1996.
- <sup>60</sup>C. Pangali, M. Rao, and B. J. Berne, *Mol. Phys.* **40**, 661 (1980).
- <sup>61</sup>L. Bosio, S. H. Chen, and J. Teixeira, *Phys. Rev. A* **27**, 1468 (1983).
- <sup>62</sup>F. Sciortino, A. Geiger, and H. E. Stanley, *Phys. Rev. Lett.* **65**, 3452 (1990).
- <sup>63</sup>G. W. Robinson, C. H. Cho, and J. Urquidi, *J. Chem. Phys.* **111**, 698 (1999).
- <sup>64</sup>R. J. Speedy and C. A. Angell, *J. Chem. Phys.* **65**, 851 (1976).
- <sup>65</sup>O. Mishima and H. E. Stanley, *Nature (London)* **396**, 329 (1998).
- <sup>66</sup>H. E. Stanley, S. V. Buldyrev, M. Canpolat, M. Meyer, O. Mishima, M. R. Sadr-Lahijany, A. Scala, and F. W. Starr, *Physica A* **257**, 213 (1998).
- <sup>67</sup>O. Mishima and H. E. Stanley, *Nature (London)* **392**, 164 (1998).
- <sup>68</sup>H. Tanaka, *J. Chem. Phys.* **105**, 5099 (1996).
- <sup>69</sup>W. L. Jorgensen and J. Tirado-Rives, *J. Phys. Chem.* **100**, 14508 (1996).
- <sup>70</sup>L. X. Dang, personal communication.